ACADEMIC PRESS

Available online at www.sciencedirect.com

SCIENCE DIRECT®

Methods 29 (2003) 14–28

METHODS

www.elsevier.com/locate/ymeth

Using FRAP and mathematical modeling to determine the in vivo kinetics of nuclear proteins

Gustavo Carrero,[a] Darin McDonald,[b] Ellen Crawford,[b] Gerda de Vries,[a] and Michael J. Hendzel[b,*]

[a] *Department of Mathematical and Statistical Sciences, University of Alberta, Alberta, Canada*
[b] *Department of Oncology, University of Alberta, Alberta, Canada*

Accepted 11 September 2002

Abstract

Fluorescence recovery after photobleaching (FRAP) has become a popular technique to investigate the behavior of proteins in living cells. Although the technique is relatively old, its application to studying endogenous intracellular proteins in living cells is relatively recent and is a consequence of the newly developed fluorescent protein-based living cell protein tags. This is particularly true for nuclear proteins, in which endogenous protein mobility has only recently been studied. Here we examine the experimental design and analysis of FRAP experiments. Mathematical modeling of FRAP data enables the experimentalist to extract information such as the association and dissociation constants, distribution of a protein between mobile and immobilized pools, and the effective diffusion coefficient of the molecule under study. As experimentalists begin to dissect the relative influence of protein domains within individual proteins, this approach will allow a quantitative assessment of the relative influences of different molecular interactions on the steady-state distribution and protein function in vivo.
© 2002 Elsevier Science (USA). All rights reserved.

Keywords: Fluorescent protein; Green fluorescent protein; Photobleaching; Fluorescence recovery after photobleaching; Nucleus; Mathematical modeling; Diffusion; Association constant; Dissociation constant; Live cell analysis; Nuclear dynamics

1. Introduction

Intracellular macromolecular mobility is influenced by specific and nonspecific interactions, diffusion, catalytic activity, and, when present, flow processes or active transport. Thus, comprehensive characterization of molecular mobility allows determination of the relative roles of each of these processes on the behavior of a biomolecule in the living cell environment. Here we review the application of fluorescence recovery after photobleaching (FRAP) and the mathematical modeling of FRAP data to the measurement of the mobility of macromolecules in living cells. Experiments that define the mobility of macromolecules undergoing both binding and diffusion events within the nucleoplasm are summarized. These experiments have allowed us to begin to understand the physical properties of the nucleoplasm [1–8], an intracellular environment about which our understanding is particularly limited. Although we emphasize the application of FRAP to the study of nuclear protein mobility, the models summarized are applicable to defining macromolecular diffusion within cellular membranes, the cytoplasm, and the nucleoplasm as well as quantifying the influences of binding and diffusion events on in vivo movement. For compartments with more complex topology, such as the Golgi and endoplasmic reticulum, alternative mathematical models are more appropriate. A discussion of the details and applications of these mathematical models is reviewed elsewhere [2] and is not discussed here. Because FRAP can be performed with laser scanning confocal microscopes, this technique is the most widely employed and available approach for measuring the movement of molecules in living cells.

* Corresponding author. Present address: Division of Experimental; Oncology, Cross Cancer Institute, 11560 University Avenue, Edmonton, Alb., Canada T6G 1Z2. Fax: +780-432-8892.
E-mail address: michaelh@cancerboard.ab.ca (M.J. Hendzel).

1046-2023/02/$ - see front matter © 2002 Elsevier Science (USA). All rights reserved.
PII: S1046-2023(02)00288-8

FRAP is a very simple technique used to measure the movement of fluorescent molecules. FRAP takes advantage of the fact that fluorescent molecules eventually lose their ability to emit fluorescence when exposed to repeated cycles of excitation and emission. This is often referred to as "photobleaching." In FRAP experiments on living cells, a subregion of the cell is photobleached to create an inhomogeneity in the cellular fluorescent population. Two populations of molecules are created that are spatially separated at the start of the experiment: the fluorescent molecules and the photobleached molecules (Fig. 1). To measure the mobility of a fluorescent molecule such as green fluorescent protein, images of the fluorescently labeled cell are collected over time while the fluorescent and photobleached molecules redistribute until equilibrium is reached. By plotting the relationship between fluorescence intensity and time, the mobility of the fluorescent proteins can be directly measured (Fig. 2).

FRAP is a relatively old technique but its application to the study of intracellular proteins in living cells is very recent and driven largely by the availability of fluorescent proteins that can be employed as cotranslational tags for proteins of interest. In the past 3 years, a number of proteins, some structural, some functional, have been investigated. Table 1 summarizes results obtained for nuclear proteins. To this point, relatively simple questions have been asked and answered using the FRAP approach. However, as we improve our capability to describe and characterize the behavior of macromolecules using increasingly complex mathematical models and experimental designs, FRAP will play

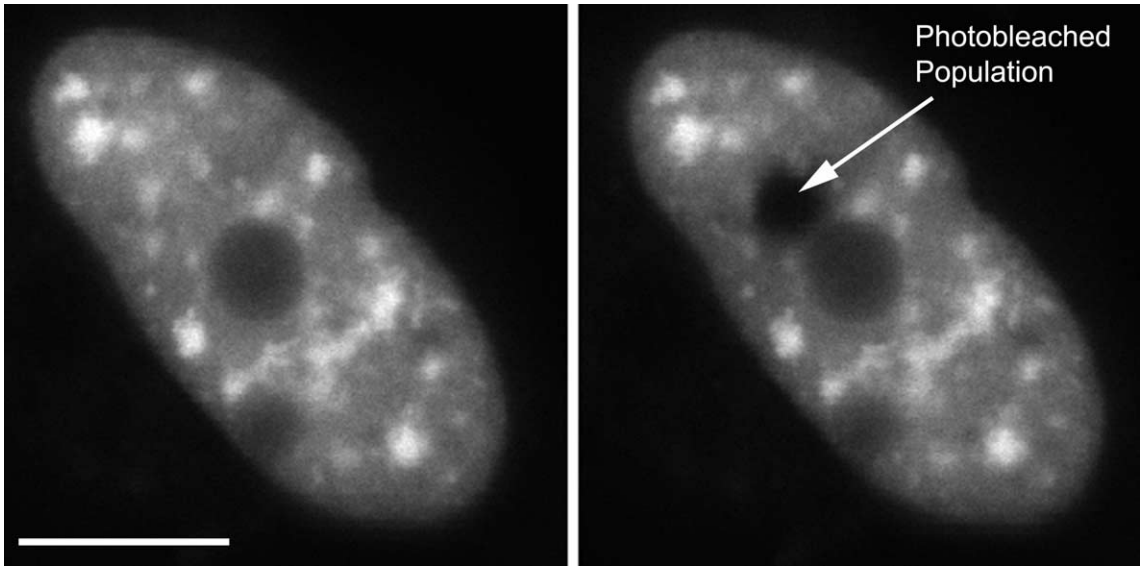

Fig. 1. Example of photobleaching. An Indian muntjac fibroblast nucleus expressing ASF/SF2-GFP is shown before (left) and after (right) photobleaching of a 2-μm spot within the nucleus. Bar = 10 μm.

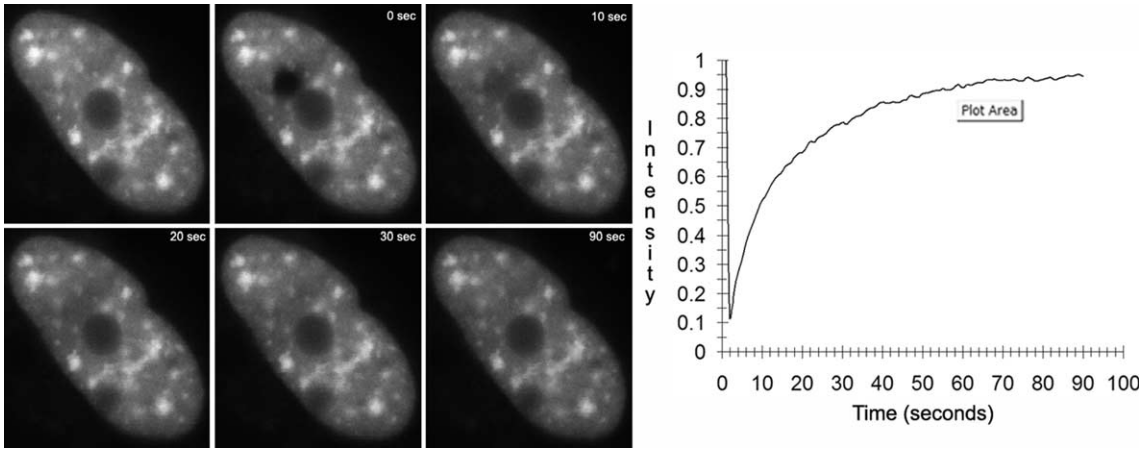

Fig. 2. Example of a FRAP recovery curve. The cell from Fig. 1 is again illustrated. Images collected at different points in the recovery time course are shown. The right-hand panel shows the normalized plot of intensity-versus-time for the cell shown.

Table 1
Nuclear protein mobility determined by FRAP

Type	GFP fusion	Measured mobility	Comments	Ref.
Nucleoplasmic	eGFP	57 μ^2/s in the nucleoplasm		[14]
	Topoisomerase II α and β	$t_{1/2}$ for 1-μm circle 6–10 s in the nucleolus, 2–3 s in the nucleoplasm	Proteins immobilized by inhibitors of topoisomerase activity	[23]
	Topoisomerase I	$t_{1/2}$ for 1-μm circle 1.1 s (nucleoplasm), 1.9 s (nucleolus); 14.3 s (nucleoplasm) and 12.5 s (nucleolus)	Two mobile fractions with distinct kinetics, enzyme relocalized and of reduced mobility when topoisomerase activity is inhibited	[24]
	ZAP-70	$>1\ \mu^2$/s (nucleoplasm)		[25]
	Protein phosphatase 1	$t_{1/2} < 30$ s (nucleolus)		[26]
	LMP2 proteosome subunit	Rapid mobility seconds time scale	Movement not inhibited by ATP depletion	[27]
Nucleoplasmic/DNA repair	XRCC1, XPA, XPB	6–15 μ^2/s in absence of UV damage	Proteins immobilized on introduction of DNA damage	[14]
	Ku70, Ku86	0.35 μ^2/s	Reduction in mobility determined by amino acids 255–550	[28]
	Rad proteins	~7.5–15 μ^2/s	Protein mobilities reduced to different extents on introduction of double-strand breaks	[29]
Nuclear body associated	ASF/SF2	0.24 μ^2/s	Mobility increased slightly on inhibition of RNA polymerase II transcription	[17] see also [30]
	Nucleolar proteins	0.019–0.16 μ^2/s in nucleolus 0.51–1.6 μ^2/s in nucleoplasm	Transcription-dependent changes in mobility observed	[31] see also [17,32]
	PML, Sp100	Mostly "immobile" over 15-min time scale	Associated with PML bodies; CBP was shown to be a dynamic component of the PML bodies under the same conditions	[33]
Chromatin associated	Histone H1	220–250 s residency time in mouse, similar in human	Both protein acetylation and protein phosphorylation alter residency times	[34,35]
	Nucleosomal histones	$t_{1/2}$ of 2 or more hours $t_{1/2} \geqslant 2$ h	H2B exchanged more rapidly than H3/H4; part of the exchanging H2B population was dependent on RNA polymerase II transcription	[36]
	HMG17	0.45 μ^2/s		[17]
Transcription factor	Stat1	Approx same as GFP		[37]
	Estrogen receptor	0.8 s—unstimulated, 6 s—stimulated	Estrogen receptor was immobilized by antagonist, ATP depletion, and inhibition of proteosome activity	[38] see also [39]
	Glucocorticoid receptor	"Rapid" seconds time scale	Stimulated receptor has short residency time on its target DNA in living cell system	[40]
	SRC-1	~10 s in presence of estradiol	Mobility reduced in ER cotransfected cells in the presence of estradiol but not other treatments, e.g., inhibitor, that reduce ER mobility	[38]

Nuclear pore	Nuclear pore protein Nup98	$t_{1/2} = 1.2$ s (nucleoplasm), 12 s (nuclear foci), >12 s in nuclear pores	Nucleoplasmic and nuclear focal populations immobilized when RNA polymerase II transcription is inhibited	[41]
	POM121	$t_{1/2} = 20$ h (nuclear pore)		[42]
	Nup153	$t_{1/2} = 15$ s	Full recovery required 4 min	[42]
Nuclear lamina/membrane	Lamin B-receptor	"Immobilized"	Diffusional in ER, very slow and incomplete recovery in nuclear membrane; mobility increased during HSV-1 expression (see [43])	[12]
	Emerin	0.1 μ^2/s (nuclear membrane)	Diffuses approximately 3-fold faster in ER	[44]
	HA-95	"Immobile" on 15-min time scale		[45]
	Lamins A, B1	"Immobile" during interphase	Lamin A is immobilized later during postmitotic nuclear reformation than lamin B1; intranuclear ("nucleoplasmic") lamins also immobilized	[46]

an increasingly important role in advancing our understanding of the behavior and function of proteins within the cytoplasm and cellular compartments such as the nucleus.

2. Description of FRAP methodology

In this section, we detail the design of, and collection of data from, a FRAP experiment. Assuming that the fluorescent tag applied to the protein under study does not inhibit function, the key principle is to balance sampling frequency with obtaining images of low noise and high dynamic range. Low-noise, high-dynamic-range images are important for sensitivity and consistency during data analysis.

2.1. Overview

The underlying principle in a FRAP experiment is that a fluorescently tagged biomolecule can be studied kinetically in living cells by examining the redistribution of the fluorescent population of molecules over space and time. FRAP is used to study the average behavior of a population of fluorescent molecules. Many copies of a desired molecular species are introduced into the cell, either using expression vectors encoding fluorescent protein tags or by tagging a purified molecule in vitro with a fluorophore and introducing it into cells by microinjection. To study the kinetic behavior of the fluorescently labeled molecules, a specific region within the cell is typically delineated using a "mask" tool. This mask defines a region that is exposed to a brief but sufficiently intense excitation pulse to irreversibly inactivate fluorescence emission. The flux of new molecules into the "photobleached" region is used as a reporter for the kinetic properties of the protein in the living cell.

Performing these experiments requires a stable light source capable of rapidly bleaching a small region of the image field and a detector for imaging the entire cell or cell nucleus during recovery. We focus on the use of a laser scanning confocal microscope to capture FRAP data. This is the most commonly available instrumentation for these experiments. Note, however, that other configurations including those that use CCD cameras can be used for FRAP [9]. Once collected, images are then quantitatively analyzed for changes in fluorescence within the photobleached region over time.

2.2. Setting up the FRAP experiment

We shall assume that the protein under study has been demonstrated to functionally substitute for the endogenous protein. When possible, this should be experimentally demonstrated prior to beginning FRAP experiments. We shall also restrict our discussion to

proteins that are introduced through transfection of proteins constructed with a fluorescent protein tag and encoded in an appropriate expression vector.

We typically transiently transfect cells and examine them 18–24 h posttransfection. Before performing any FRAP experiments, we confirm that the transfected protein recapitulates the endogenous protein distribution. Some proteins will not show a steady-state distribution in living cells that reflects the distribution of the endogenous protein. In our experience, two types of artifactual distributions are commonplace: (1) diffuse distribution without the expected enrichment in steady-state compartments and (2) the formation of large spherical aggregates. Examples of these distributions are illustrated for histone deacetylase–GFP fusion proteins (Fig. 3). Proteins that behave in this manner are not appropriate for analysis unless immunofluorescence of the endogenous protein indicates that this is the normal steady-state distribution.

To establish photobleaching conditions, fix transfected cells with 4% paraformaldehyde in PBS, pH 7.2, for 5 min at room temperature. Mount the coverslip in cell culture medium and mount the slide on the confocal microscope. Using a mask tool, define a small subregion to be photobleached. Typically, a diffraction-limited spot is photobleached. However, because of the frame rate limitations on many current confocal microscopes, larger circles of up to 2-μm diameter or more may be required to adequately capture the diffusional phase of recovery for even relatively large proteins [10]. Once a region has been defined, determine: (1) the minimum number of iterations at maximum laser power required to photobleach the defined region to background fluorescence levels and (2) that there is no evidence of fluorescence recovery in the photobleached region several minutes after photobleaching the fixed cell. This is done to minimize the time that it takes to photobleach the region and to determine that the photobleaching is irreversible. It is important to photobleach the specimen as rapidly as possible because there will otherwise be significant redistribution during the photobleaching process of photobleached and fluorescent molecules initially outside of the photobleached region. When this occurs, the first image scan after photobleaching will reveal an overall decrease in fluorescence intensity rather than a defined photobleached region.

2.2.1. Cell culture conditions during FRAP

It is important, of course, that cells are healthy during the photobleaching experiment. To obtain optimal growth conditions during imaging, both objective and stage heaters are required to maintain temperature at 37 °C and carbon dioxide needs to be maintained at 5%. Because energy-dependent processes are significantly more sensitive to temperature-dependent changes in mobility than energy-independent processes such as diffusion, simply performing a FRAP experiment at 22 and 37 °C will allow you to identify energy-dependent events. Although molecular diffusion is also influenced by temperature, a 15-K change in absolute temperature results in a decrease in diffusion rate that is too small to be resolved by FRAP.

Most proteins have mobilities that are not energy-dependent [4,6–8,11]. Consequently, very simple culture

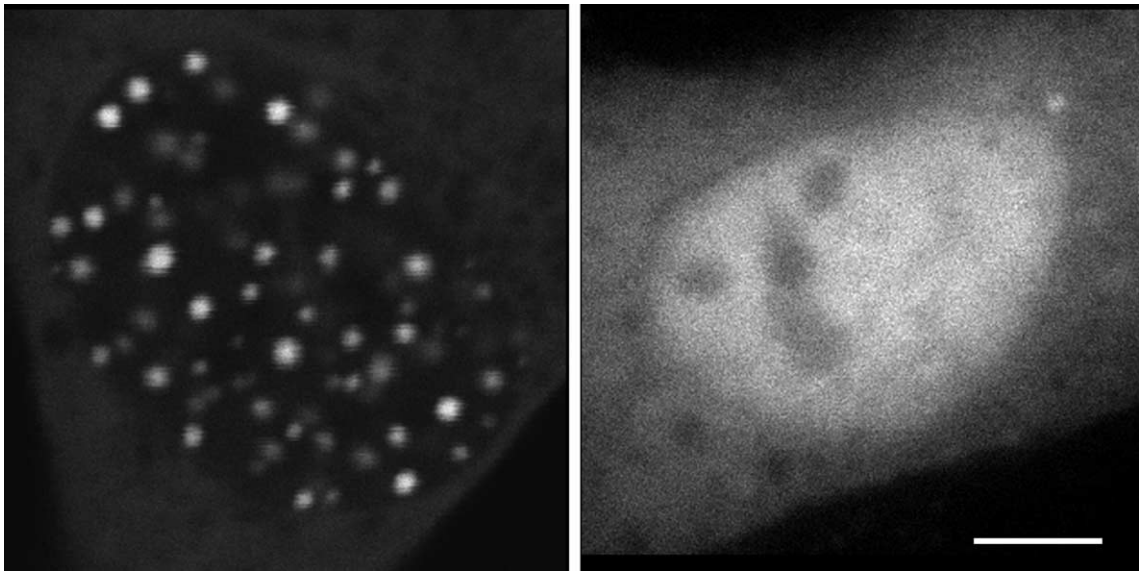

Fig. 3. Abnormal distributions of GFP-tagged histone deacetylases. Mouse $10t_{1/2}$ cells transfected with either HDAC4-GFP (left) or HDAC3-GFP (right) are illustrated. Left: Numerous spherical domains are scattered throughout the nucleoplasm. These domains are significantly larger than the typical foci observed for histone deacetylases. Right: The tagged histone deacetylase does not properly localize to foci. The diffuse distribution with the only evident structure being the nucleoli is not typical of the endogenous protein. The GFP tag disrupts localization in this instance. Bar = 5 μm.

conditions can be set up on a microscope slide. We make an approximately 1-mm-deep "well" on a glass slide using vacuum grease, place a couple of drops of medium in the well, and then mount the coverslip with the cells facing the medium. We then perform our experiments at either 22 or 37 °C. We use each slide for up to 2 h before mounting another. The pH of the culture is maintained over this period.

While phototoxicity is often expressed as a concern because "high-intensity" illumination is used to photobleach the protein under study, photobleaching is generally not phototoxic under typical experimental conditions [4]. For example, Ellenberg and colleagues have studied the behavior of nuclear pores over the course of more than 24 h without phototoxicity [12]. Thus, on the time scale of minutes, the duration required for most FRAP experiments, phototoxicity concerns can be dismissed. A simple means of verifying this under your conditions is to return the coverslip to the cell culture incubator after the experiment and examine the photobleached cells over the 24–48 h following the photobleaching experiment to determine whether they have a normal morphology, have undergone cell division, or show signs of apoptosis. If cells have undergone cell division, this is a strong indicator that there are negligible phototoxicity issues under your experimental conditions.

2.3. Pilot experiments to determine frame rate and experiment duration

Once it has been established that the fusion protein properly associates with the appropriate steady-state compartments within the cell, the next step is to determine the optimal time interval between data points (images) during the recovery phase of the experiment. Table 1 shows the diffusion coefficients for several nuclear proteins that have been measured. Most nuclear proteins have mobilities that are considerably slower than expected for free diffusion and will require experiments of several (typically 2–5) min to reequilibrate fluorescence following the photobleaching of a 2-μm-diameter spot or strip.

We typically perform a pilot experiment by following the recovery of a photobleached spot at 5- to 10-s intervals over approximately 2 min. The uncorrected (raw data) plot of intensity-versus-time is then evaluated for: (1) the extent of recovery during the first 5 s of recovery and (2) the duration of time required to achieve a plateau in the recovery curve. The extent of recovery during the first 5 s, if substantial, represents the free-diffusion phase for proteins moving through the aqueous phase of the cell. Integral membrane proteins diffuse a couple of orders of magnitude slower than this [10]. When a significant freely diffusing population is present, we sample the first 5 s of the recovery phase as rapidly as possible. Ideally, we try to obtain at least five data points in the first 5 s. We determine the duration of the experiment by identifying the time required for recovery to reach completion in the intensity-versus-time plot of the "raw data." We then extend the duration of the experiment approximately 30% longer than the time required to equilibrate. For analysis with a compartmental model (see next section), we extend this duration to double the length of time required to equilibrate. This is required for more accurate quantification of binding events.

2.4. Collecting the data

We typically aim to collect approximately 50 data points over the course of the recovery curve. This is sufficient to identify individual populations while minimizing photobleaching during the collection of the recovery images. When both fast and slow migrating populations are present, we increase the interval between images following the first 5- to 10-s of recovery to enable longer time scales to be sampled with the same 50 data points. We also typically sample spatially at 100 nm/pixel *xy* resolution and open the pinhole aperture of the confocal microscope to optimize light collection rather than to optimize optical section thickness. The short residency time of the detector at each pixel during image scanning can lead to signal-to-noise ratio problems. Significant amounts of noise will make it impossible to reliably determine the percentages of the protein found in mobile and immobile pools. Hence, image collection is optimized to balance high signal-to-noise ratio images with sufficiently low illumination during the recovery phase to avoid greater than 10–20% fluorescence loss through photobleaching over the course of the recovery curve.

2.5. Normalizing data for quantification

The "raw" fluorescence intensity-versus-time curves are not suitable for direct quantitative analysis. Rather, the data must be normalized to correct for: (1) the background signal in the image, (2) the loss of total cellular fluorescence that arises from photobleaching a subregion of the cell, and (3) any loss of fluorescence that occurs during the course of collection of the recovery time series. Thus, on each image series, we collect intensity information on the photobleached region, the total cellular fluorescence, and the background signal obtained from a region not containing fluorescent protein. When data export procedures are used to generate consistently organized columns of data, it is convenient to write a simple macro in MS Excel or similar software to automatically perform data normalization routines on raw data.

The experimental fluorescence recovery data of a photobleached region, recorded at times t_j, with $1 \leqslant j \leqslant n$,

can be presented in two forms: normalized with respect to the fluorescence intensity in the bleached region before photobleaching, $F^*(t_j)$; or normalized with respect to the final fluorescence intensity in the bleached region, $\overline{F}(t_j)$. The difference is that in the first case the proportion of the fluorescence intensity lost due to photobleaching is exhibited, and therefore, the normalized data will not reach unity, i.e., $F^*(t_n) < 1$, whereas in the second case this loss is not exhibited, and consequently, $\overline{F}(t_n) = 1$. The importance of this difference will become apparent later.

2.6. What to expect

Intracellular diffusion has been studied using inert transiently expressed or microinjected biomolecules [13,14]. In these instances, diffusion coefficients can be estimated and compared with the diffusion coefficient of the molecule in water [2]. The studies that have been performed to date enable us to draw some conclusions about the biophysical properties of both the cytoplasm and the nucleoplasm. First, the density of obstacles to diffusion within the aqueous phase of the cell is sufficiently high that anomalous diffusion occurs [2,15]. Anomalous diffusion is where the mean squared displacement of a protein molecule deviates from linearity with time in contrast to true diffusion, where the mean squared displacement is linearly dependent on time. Second, there appears to be an upper limit to the size of molecule that can freely diffuse within the cell [2]. Inert molecules as small as 2 MDa have been observed to be significantly immobilized when microinjected into the nucleoplasm [13]. Despite compositional differences between the nucleoplasm and the cytoplasm, both have very similar physical properties with respect to diffusion. Third, although some proteins such as GFP can diffuse through the cell at rates only approximately fourfold slower than in dilute solution, the majority of biologically active nuclear proteins that have been studied migrate at rates two orders of magnitude slower than free diffusion (Table 1).

3. Analyzing the data

In this section, we examine different ways to analyze the data. Depending on the purpose of the experiment, simple measurements such as the half-time of recovery may be sufficient to describe the relative protein behavior. Mathematical modeling to fit simulated curves to experimental data is required if more biologically meaningful numbers are to be extracted. The most commonly used approach to describe the mobility of nuclear proteins during FRAP experiments is to assume the spatiotemporal dynamics of these proteins to be diffusive in nature. Under this assumption, the kinetic parameter that measures the rate of movement, and reflects the mean squared displacement explored by the proteins through a random walk over time, is the diffusion coefficient. Because the simple diffusion equation does not take into consideration any kind of interaction that nuclear proteins might be undergoing, the measurement obtained has been more appropriately termed the *effective* diffusion coefficient [4] or *apparent* diffusion coefficient [6], which indicates the overall measure of the parameter.

The first part of this section is devoted to summarizing the underlying mathematical analysis that allows one to estimate an effective diffusion coefficient, and to assess the influence of the nuclear membrane on diffusion. We examine models for diffusion within theoretical "infinite domains" as well as models that account for the membrane-bounded topology of the cell, the nucleus, or other cellular compartments. The second part of this section incorporates into the mobility analysis binding and unbinding events and shows how different approaches allow estimation of the dynamical parameters describing molecular interactions. The uses and assumptions of each model described are summarized in Table 2.

3.1. Standard methodology using a simple 2D model for diffusion

The standard method for estimating an effective diffusion coefficient is based on the work of Axelrod et al. [16], where it is assumed that the photobleaching is performed on a two-dimensional region that has reached a homogeneous steady-state distribution of fluorescent species and that the movement of molecules is governed by a simple random walk on an infinite (unbounded) domain. Although this model was originally applied to the *2D* diffusion of proteins within biological membranes, it has been extensively used to obtain an effective mobility measurement for *3D* diffusion within the cytoplasm and nucleoplasm.

The diffusion model of Axelrod assumes that the concentration of fluorescent species $u(\boldsymbol{x}, t)$ after photobleaching at position $\boldsymbol{x} = (x, y)$ and time t can be represented by the simple diffusion equation

$$\begin{aligned} &\frac{\partial}{\partial t} u(\boldsymbol{x}, t) = D_{\text{eff}} \Delta u(\boldsymbol{x}, t), \quad t > 0, \\ &u(\boldsymbol{x}, 0) = f(\boldsymbol{x}), \end{aligned} \tag{1}$$

where Δ denotes the Laplacian operator, i.e.,

$$\Delta u = \frac{\partial^2 u}{\partial x^2} + \frac{\partial^2 u}{\partial y^2},$$

D_{eff} is the effective diffusion coefficient, and $f(\boldsymbol{x})$ is the initial condition of fluorescent species right after photobleaching. This initial condition depends on the intensity profile $I(\boldsymbol{x})$ of the laser beam that is used to

Table 2
Summary of mathematical models

Model	Reference	Measurements	Assumptions	Strengths	Limitations
Diffusion equation (1)	[16]	Effective diffusion coefficient D_{eff}	Dimension: 2D	A simple expression [Eq. (6)] for calculating D_{eff} is available.	Does not account for the existence of a boundary
			Domain: Unbounded infinite		Can lead to slightly erroneous estimations of D_{eff} if region photobleached is large in relation to the size of the domain
			Photobleaching profile: Gaussian or circular	The solution gives an explicit theoretical fluorescence recovery curve [Eq. (3)] to fit the data	Does not account for molecular interactions
Diffusion equation (8)	[47]	Effective diffusion coefficient D_{eff}	Dimension: 2D	The model considers a bounded domain	The model is solved explicitly only when photobleaching is performed in the center of the disk
			Domain: bounded A disk	A simple expression [Eq. (7)] for calculating D_{eff} is available	Does not account for molecular interactions
			Photobleaching profile: Gaussian		
Diffusion equation (8)	[19]	Effective diffusion coefficient D_{eff}	Dimension: 2D	The model considers a bounded domain	The model is solved explicitly only when photobleaching is performed in the center of the rectangle
			Domain: bounded rectangle		
			Photobleaching profile: Gaussian		Does not account for molecular interactions
Diffusion equation (8)	Unpublished results	Effective diffusion coefficient D_{eff}	Dimension: 2D	The model considers a bounded domain	Photobleaching profile is approximated with a rectangle
			Domain: bounded rectangle	The solution shows explicitly the influence of the photobleaching location	Does not account for molecular interactions
			Photobleaching profile: rectangular		
Diffusion equation (9)	Present work	Effective diffusion coefficient D_{eff}	Dimension: 2D reduced to 1D	The model considers a bounded domain	
			Domain: bounded rectangle reduced to a segment	The model is reduced to 1D	Photobleaching profile has to be a narrow band
			Photobleaching profile has to be a narrow band	The solution [Eq. (11)] shows explicitly the influence of the photobleaching location	Does not account for molecular interactions
Diffusion equation (1)	Present work	Effective diffusion coefficient D_{eff}	Dimension: 2D reduced to 1D		Does not account for the existence of a boundary
			Domain: unbounded infinite		Can lead to slightly erroneous estimations of D_{eff} if region photobleached is large in relation to the size of the domain
			Photobleaching profile: narrow band	The solution gives an explicit theoretical fluorescence recovery curve [Eq. (12)] to fit the data	Does not account for molecular interactions
					Photobleaching profile has to be a narrow band

Table 2 (*continued*)

Model	Reference	Measurements	Assumptions	Strengths	Limitations
Reaction–diffusion equation (15)	[20]	Diffusion coefficient Δ Binding association rate k_a	Dimension: 2D reduced to 1D Domain: bounded rectangle reduced to a segment Photobleaching profile: narrow band	The model accounts for binding and unbinding events A more realistic diffusion coefficient is obtained	The complicated nature of the solution brings difficulty to the estimation of the parameters D, k_a, and k_d
		Unbinding dissociation rate k_d	Immobile structure to which the biomolecules are bound is homogeneously distributed	The solution explains fast and slow phases of recovery curves	
Compartmental model (16)	Present work	Binding association rate k_a	Domain: actual physical domain	The model considers implicitly the space	The model is not designed to estimate a diffusion coefficient since space is not considered explicitly
		Unbinding dissociation rate k_d	Photobleaching profile: narrow band	The model is a simple system of linear ordinary differential equations The solution [Eq. (19)] used to fit the FRAP data is a simple exponential sum	

photobleach a certain region Λ. Therefore, according to Eq. (6) in [16], the theoretical recovery curve is given by

$$F(t) = \frac{q}{A}\int_{\Lambda} I(\boldsymbol{x})u(\boldsymbol{x},t)\,\mathrm{d}x, \tag{2}$$

where q is the product of all the quantum efficiencies of light absorption, emission, and detection and A is the attenuation factor of the laser beam during observation of recovery [17]. Axelrod et al. solved Eq. (1) using a Gaussian intensity profile, obtaining in this way the following explicit theoretical fluorescence recovery curve, which can be used to fit the normalized data $\overline{F}(t_j)$,

$$F(t) = \sum_{N=0}^{\infty} \frac{(-K)^N}{N!}\left[1 + N\left(1 + \frac{2t}{\tau_{D_{\mathrm{eff}}}}\right)\right]^{-1}, \tag{3}$$

where $\tau_{D_{\mathrm{eff}}} = w^2/(4D_{\mathrm{eff}})$ is the characteristic diffusion time, w is the half-width of the intensity at e^{-2} height, and K is a parameter describing the amount of bleaching (see [16] for details).

Note that w and K are parameters that characterize the bleaching profile of the laser beam, and that their values can be obtained directly from experimental data. To do so, a spot of a fixed specimen, with an initial uniform fluorophore concentration C_i, is photobleached under the same conditions used in the experiment. From the image of the photobleached chemically fixed specimen, one can extract the fluorescence intensity data as a function of distance r from the center of the bleached spot. These data can be fitted with the equation that describes the irreversible reaction of the photobleaching (Eq. (1) in [16]):

$$C_u(r) = C_i \exp[-K\exp(-2r^2/w^2)], \tag{4}$$

where $C_u(r)$ is the concentration of unbleached fluorophore as a function of radial distance. By fitting the data with the method of least squares [18], w and K can be estimated simultaneously. Moreover, this fitting could be simplified if one first estimates K from the initial fluorescence (Eq. (7) in [16]),

$$F(0) = K^{-1}(1 - e^{-K}), \tag{5}$$

and then applies least squares to obtain an estimation for w.

Thus, the only parameter left to be estimated in Eq. (3) is the effective diffusion coefficient D_{eff}. This estimation can be obtained directly by fitting formula (3) to the data, using the method of least squares. Phair and Misteli [17] used this approach to estimate effective diffusion coefficients for several nuclear proteins. Alternatively, one could estimate the effective diffusion coefficient using the following formula proposed by Axelrod et al. (Eq. (19) in [16]),

$$D_{\mathrm{eff}} = \frac{w^2}{4\tau_{1/2}}\gamma, \tag{6}$$

where $\tau_{1/2}$ is the time for half-recovery and γ is a correction factor that can be obtained in terms of K (see [16] for details).

This standard technique to estimate coefficients of diffusion for cellular molecules assumes that the diffusion process occurs on an infinite domain. Thus, the estimates for D_{eff} can be considered accurate in the cases where the photobleached region is a small fraction of the cell or cellular compartment under study. However, the method ignores the fact that any cellular membrane is a diffusional boundary for most of the proteins under study. Wey and Cone [47] solved the diffusion equation on a finite domain (a disk) and found that the formula analogous to Eq. (6) for estimating an effective diffusion coefficient, when photobleaching in the center with a Gaussian profile, is (Eq. (2) in [47]),

$$D_{\text{eff}} = \frac{fR^2}{\tau_{1/2}\pi^2}, \tag{7}$$

where R is the disk radius, and f is a function of R and w, the half-width of the intensity at e^{-2} height. Therefore, the estimation of a diffusion coefficient on a bounded domain can be inaccurate if an infinite domain is assumed in the analysis. The issue of FRAP experiments in bounded regions was also addressed by Angelides et al. [19], who asserted the dependence of fluorescence recovery curves after photobleaching on the size and shape of the area available for diffusion. Specifically, they simulated fluorescence recovery curves on rectangular domains of different dimensions, obtaining in this way curves with different asymptotic behaviors (see [19] for details).

3.2. Estimating diffusion within a membrane-bounded domain

Membranes are common diffusional barriers within cells. To obtain theoretical insight into the influence of membrane barriers to diffusion on the estimation of diffusion coefficients in FRAP experiments, and to derive a simple theoretical fluorescence recovery curve that could be used to fit experimental data on finite domains, we introduce a boundary into model (1). By doing so, and assuming that there is no flux of fluorescent biomolecules into or out of the cell or cellular compartment during the time scale of the experiment, the diffusion model (Eq. (1)) becomes an initial boundary-value problem subject to Neumann (no-flux) boundary conditions:

$$\begin{aligned}
&\frac{\partial}{\partial t}u(\boldsymbol{x},t) = D_{\text{eff}}\Delta u(\boldsymbol{x},t), \quad \boldsymbol{x}\in\Omega,\ t>0,\\
&\frac{\partial u}{\partial \eta} = 0, \quad \boldsymbol{x}\in\partial\Omega,\ t>0,\\
&u(\boldsymbol{x},0) = f(\boldsymbol{x}), \quad \boldsymbol{x}\in\Omega,
\end{aligned} \tag{8}$$

where Ω represents the cell or cell compartment, $\partial\Omega$ its boundary, i.e., its membrane, and η is the outer unit vector normal to the boundary. Although we developed and discuss this model for estimating the diffusion of proteins within the nucleus, the underlying principles hold for any definable diffusional boundary within the cell.

To solve Eq. (8) explicitly, we approximate the shape of the nucleus with a rectangle of length l. Since a narrow band is a common photobleaching profile in FRAP experiments on bounded domains [20,21], we model the photobleached region as a narrow band of width $2h$, and centered on the x axis at c (Fig. 4). With these assumptions, the problem can be reduced to one dimension, i.e., Eq. (8) becomes

$$\begin{aligned}
&\frac{\partial}{\partial t}u(x,t) = D_{\text{eff}}\frac{\partial}{\partial x^2}u(x,t), \quad x\in(0,l),\ t>0,\\
&\frac{\partial u}{\partial x} = 0, \quad x=0,l,\ t>0,\\
&u(x,0) = f(x), \quad x\in(0,l),
\end{aligned} \tag{9}$$

where the initial condition is given by

$$f(x) = \begin{cases} 0, & |x-c| \leqslant 0,\\ u_0, & |x-c| > 0, \end{cases} \tag{10}$$

and u_0 is the initial uniform steady-state concentration of the fluorescent biomolecule before photobleaching. Note that the above initial condition does not describe a Gaussian photobleaching profile, but a uniform profile that can be interpreted as an approximation of a Gaussian profile with a large amount of bleaching induced by the laser beam, i.e., $K \gg 1$. Tardy et al. [20] and McGrath et al. [21] also have used this kind of initial condition to model the photobleaching of a band in FRAP experiments examining the dynamics of cytoplasmic actin.

By integrating the solution of Eq. (9) over $2h$, dividing this result by the total population of fluorescent

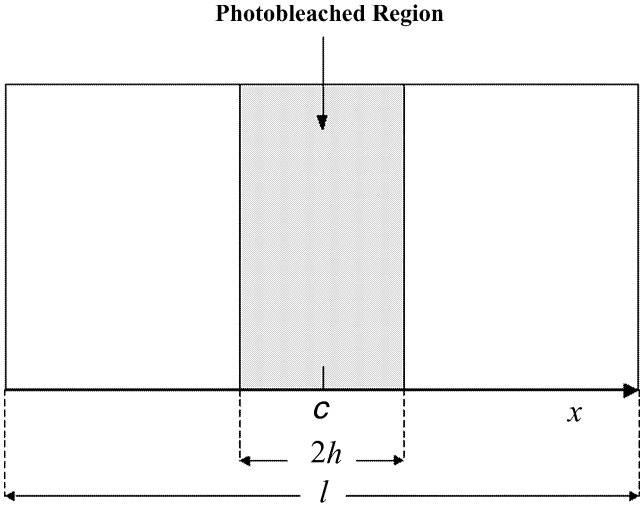

Fig. 4. Geometrical assumption for the cell nucleus. The shape of the cell nucleus is approximated with a rectangle of length l, and the photobleached region is modeled as a narrow band of width $2h$, centered on the x axis at c.

biomolecules in the photobleached region, $2hu_0$, and assuming that the fluorescence intensity is proportional to the concentration of fluorescent biomolecules, a theoretical fluorescence recovery curve is obtained:

$$F_{\mathrm{B}}(t) = \frac{(l-2h)}{l} - \frac{l}{h\pi^2}\sum_{n=1}^{\infty}\frac{1}{n^2}\mathrm{e}^{-(n\pi/l)^2 D_{\mathrm{eff}}t} \times \left[\sin\left(\frac{n\pi(c-h)}{l}\right) - \sin\left(\frac{n\pi(c+h)}{l}\right)\right]^2. \quad (11)$$

In practice, if Eq. (11) were to be used to estimate a diffusion coefficient on a bounded region, it is important to photobleach the band as closely as possible to the center of the cell or cellular compartment under study and to estimate the longitude l in terms of the fluorescence intensity of the region before photobleaching, F_0, and right after photobleaching, F_{a}. Specifically, $l = 2h(F_0/(F_0 - F_{\mathrm{a}}))$.

If the photobleaching profile were described by a square instead of a band, a formula analogous to Eq. (11) can be obtained in two dimensions, but the details are beyond the scope of this article.

To assess the influence of the membrane on the estimation of diffusion coefficients, we also solve the diffusion equation, Eq. (9), on an infinite domain using the same initial condition. In this case, the theoretical fluorescence recovery curve is given by

$$F_{\mathrm{U}}(t) = \frac{1}{4h}\int_{-h}^{h}\left[\mathrm{erfc}\left(\frac{h+x}{\sqrt{4D_{\mathrm{eff}}t}}\right) + \mathrm{erfc}\left(\frac{h-x}{\sqrt{4D_{\mathrm{eff}}t}}\right)\right]\mathrm{d}x, \quad (12)$$

where $\mathrm{erfc}(x) = 1 - (2/\sqrt{\pi})\int_0^x e^{-v}\mathrm{d}v$ is the error function complement.

To illustrate the influence of the nuclear membrane and understand some theoretical aspects that one should bear in mind when interpreting estimated diffusion coefficients, we compare the fluorescence recovery curve on a bounded domain, Eq. (11), with the recovery curve on an unbounded domain, Eq. (12). We focus on two important differences. The first difference is that the rate of fluorescence recovery on a bounded domain depends on the location of the photobleaching, whereas on an unbounded domain does not. In particular, on a bounded domain, the closer to the boundary the photobleaching is performed, the slower the rate of fluorescence recovery (Fig. 5). We have observed this experimentally while studying the diffusion of Creb binding protein (CBP) within the nucleoplasm (unpublished observations). The second difference is that the asymptotic behavior of the fluorescence recovery curves is different. More concretely,

$$\lim_{t\to\infty} F_{\mathrm{B}}(t) = \frac{l-2h}{l} < 1, \quad \text{and} \quad \lim_{t\to\infty} F_{\mathrm{U}}(t) = 1. \quad (13)$$

In other words, the theoretical recovery on a bounded domain simulates the loss of fluorescence, whereas this is not the case on an infinite domain.

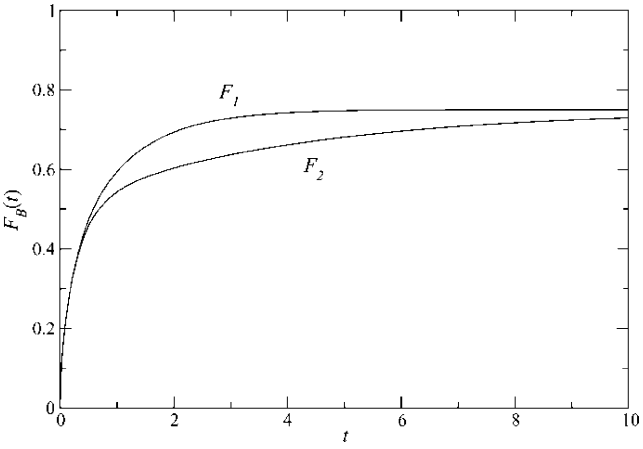

Fig. 5. Dependence of fluorescence recovery curves on the location of the photobleaching. Curves F_1 and F_2 are obtained using Eq. (11) on a rectangular domain of length $l = 20\,\mu\mathrm{m}$, with an effective diffusion coefficient $D_{\mathrm{eff}} = 10\,\mu\mathrm{m}^2/\mathrm{s}$, and a photobleached narrow band of width $2h = 5\,\mu\mathrm{m}$. For F_1, the photobleached band is centered on the x axis at $c = l/2 = 10\,\mu\mathrm{m}$, and for F_2, the photobleached band is centered closer to the boundary at $c = l/4 = 5\,\mu\mathrm{m}$.

Let us see how this fact can lead to slight overestimations or underestimations of D_{eff}. Suppose that a FRAP experiment is performed in the cell nucleus with an estimated length $l = 20\,\mu\mathrm{m}$, where a centered band of width $2h = 5\,\mu\mathrm{m}$ is photobleached. The fluorescence recovery data obtained from the experiment can be presented normalized with respect to the *initial* fluorescence before photobleaching, $F^*(t_j)$, as shown in Fig. 6A, or normalized with respect to *final* fluorescence intensity, $\overline{F}(t_j)$, as shown in Fig. 6B.

In Fig. 6A, we fit the data $F^*(t_j)$ with the theoretical recovery curve $F_{\mathrm{B}}(t)$ (Eq. (11)) using the method of least squares [18], to obtain an effective diffusion coefficient $D_{\mathrm{eff}} = 10\,\mu\mathrm{m}^2/\mathrm{s}$. To fit the data in Fig. 6B, we use the normalized recovery curve

$$\overline{F}_{\mathrm{B}}(t) = \frac{F_{\mathrm{B}}(t)}{(l-2h)/l}. \quad (14)$$

Since this fitting is equivalent to the fitting shown in Fig. 6A, we again obtain $D_{\mathrm{eff}} = 10\,\mu\mathrm{m}^2/\mathrm{s}$.

In both Figs. 6A and B, we show the fluorescence recovery curve on an infinite domain $F_{\mathrm{U}}(t)$ (Eq. (12)), corresponding to an effective diffusion coefficient $D_{\mathrm{eff}} = 10\,\mu\mathrm{m}^2/\mathrm{s}$. We note that the recovery curve on an infinite domain F_{U} lies *above* the experimental data in Fig. 6A, whereas it lies *below* it in Fig. 6B. Therefore, if the data $F^*(t_j)$ depicted in Fig. 6A were fitted with the theoretical recovery curve on an infinite domain (Eq. (12)), then the curve F_{U} in Fig. 6A would have to be lowered, meaning that the effective diffusion coefficient would be *underestimated*. On the other hand, if the data were presented as $\overline{F}(t_j)$, as depicted in Fig. 6B, and were fitted with the theoretical recovery curve on an infinite domain, then the curve F_{U} in Fig. 6B would have to be

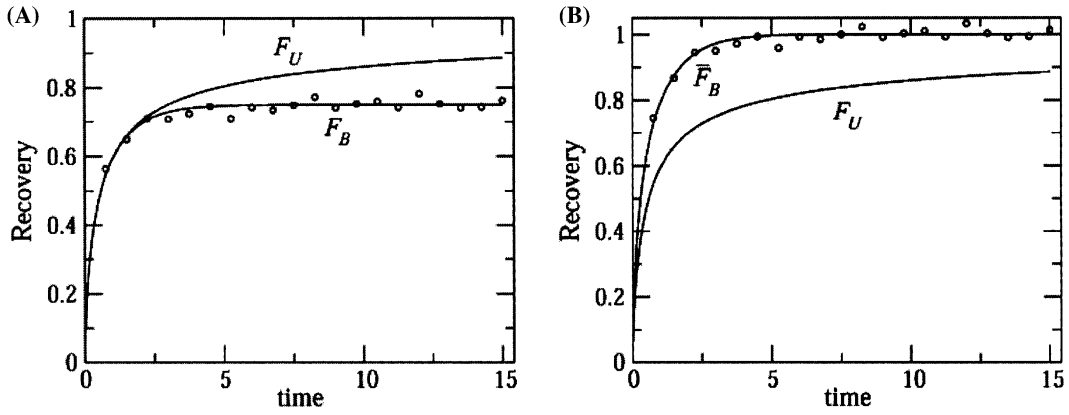

Fig. 6. Assessment of the influence of the nuclear membrane in the case of photobleaching of a narrow band of width $2h = 5\,\mu m$ on a cell nucleus approximated with a rectangular domain of length $l = 20\mu m$. The small circles represent the simulated experimental data. (A) Fitting process when the experimental data are presented normalized with respect to the fluorescence intensity in the bleached region *before* photobleaching. The small circles represent the simulated experimental data presented as $F^*(t_j)$. These data are fitted with F_B [Eq. (11)], obtaining an estimated effective diffusion coefficient $D_{eff} = 10\,\mu m^2/s$. F_U is the recovery curve on an infinite domain corresponding to the estimated diffusion coefficient $D_{eff} = 10\,\mu m^2/s$. (B) Fitting process when the experimental data are presented normalized with respect to the *final* fluorescence intensity in the bleached region. The small circles represent the same simulated experimental data as shown in Fig. 6A, but now presented as $\overline{F}(t_j)$. These data are fitted with $\overline{F}_B(t) = [F_B(t)]/[(l-2h)/l]$ [Eq. (14)], obtaining, as in (A), an estimated effective diffusion coefficient $D_{eff} = 10\,\mu m^2/s$. F_U is the recovery curve on an infinite domain corresponding to the estimated diffusion coefficient $D_{eff} = 10\,\mu m^2/s$.

lifted, meaning that the effective diffusion coefficient would be *overestimated*.

From Fig. 6A, we note that initially, the recovery curve corresponding to a bounded domain is indistinguishable from the one on an infinite domain. Biophysically, this means that initially the role of the boundary in negligible. Thus, in the case of Fig. 6A, the underestimation could be avoided by fitting only the initial set of the data.

In conclusion, the simple process of estimating an effective diffusion coefficient has subtleties, which if borne in mind, will result in a better understanding of the qualitative and quantitative results of FRAP experiments.

3.3. Quantifying molecular interactions in vivo using FRAP

Although analyzing the mobility of proteins by obtaining a measure of the *effective diffusion coefficient* has been useful in generating an appreciation for the efficiency of energy-independent diffusional processes in distributing molecules throughout the cell, it offers very little in terms of defining biological functionality. Unlike cytoplasmic proteins, which are predominantly spatially confined by membranes that bound intracellular compartments, most functional nuclear proteins interact with structures (e.g., chromatin, nuclear speckles, and nucleoli) that are essentially immobile on the time scale of molecular movement. These interactions either may be involved in the performance of a catalytic or structural role in a biological process or may be a result of sequestration into compartments that function to regulate the nucleoplasmic availability of specific nuclear proteins. Although diffusion is responsible for redistributing these functional biomolecules once they dissociate from their binding sites, the binding event itself is the primary determinant of the rate of a protein's movement through the nucleoplasm. With appropriate mathematical models, FRAP can be used to quantify these molecular interactions and obtain association and dissociation constants. This section discusses the use of mathematical models to obtain quantitative information on binding events and focuses on nuclear proteins. However, the models discussed are broadly applicable to any molecule that undergoes interactions with structures large enough to be immobile on the time scale of the typical FRAP experiment. Macromolecular assemblies of proteins involved in intracellular signaling events initiated beneath receptor clusters located on the plasma membrane, for example, would represent this class of interaction.

If one wants to describe the dynamics of diffusive biomolecules in the cell nucleus that undergo a reversible process of binding and unbinding with a structure that can be assumed to be immobile and homogeneously distributed, then one can include the effect of this reversible process in the diffusion model Eq. (8), obtaining in this way the following broadly known system of reaction–diffusion equations in [22] (Eqs. [14.62]–[14.63]),

$$\begin{aligned} \frac{\partial}{\partial t}u_f &= D\frac{\partial^2}{\partial x^2}u_f - k_a u_f + k_d u_b, \\ \frac{\partial}{\partial t}u_b &= k_a u_f - k_d u_b, \end{aligned} \tag{15}$$

where u_f and u_b represent the populations of biomolecules free to diffuse and bind to the immobile structure, respectively, D is the diffusion coefficient, k_a and k_d represent the binding and unbinding rates, respectively, t

represents time, and x is the spatial coordinate of position along a domain.

Note that Eq. (15) is presented as a one-dimensional system. Thus, if this equation were to be used to estimate dynamical parameters in FRAP experiments on a two-dimensional domain, then the appropriate photobleaching laser profile to be used is a narrow band (Fig. 4) to reduce the problem to one dimension. This procedure was followed by Tardy et al. [20] and McGrath et al. [21] when they applied Eq. (15) in the context of cytoplasmic actin dynamics. More concretely, they approximated the cell with a rectangular shape, and considered two populations of actin that depend explicitly on space and time: an immobile population of actin molecules in a filamentous form u_b, and a diffusing monomeric population u_f. They described the interaction between these populations by an association rate k_a of monomers to the filamentous pool, and a dissociation rate k_d of monomers from the filaments.

With appropriate initial and boundary conditions, an explicit solution of Eq. (15) can be found (Eq. (12) in [20]). The solution is a complicated expression that is given as an infinite Fourier series, where the three parameters to be estimated (D, k_a, and k_d) with FRAP or PAF (photoactivated fluorescence) experiments appear within long nonlinear terms.

The main importance of Eq. (15) stems from the fact that it can describe a fast phase in FRAP or PAF curves, termed "diffusion regime" [20], and a slow phase, termed "turnover regime" [20]. However, there is a lack of simplicity in the process of estimation of parameters due to the complicated nature of the explicit solution of the model (Eq. (12) in [20]).

For this reason, we suggest the use of compartmental modeling, which simplifies the task of estimating the parameters k_a and k_d by fitting the experimental data with a theoretical fluorescence recovery curve that is expressed as a simple exponential sum. The nature of this exponential sum function will also explain the slow and fast phases of the recovery curve.

Similarly to Eq. (15), the proposed compartmental model assumes two interacting populations of biomolecules that depend explicitly only on time, u_f and u_b, which represent the population of biomolecules free to diffuse, and the population of biomolecules bound to the immobile structure, respectively. When performing a photobleaching of a narrow band, the two populations occupy three physical compartments within the cell nucleus, namely, the photobleached band C_0, the left unbleached region C_1, and the right unbleached region C_2, as shown in Fig. 7A. These compartments do not represent recognized structures (e.g., "speckles" in the kinetic model presented by Phair and Misteli in [17]), but simply physical compartments dictated by the photobleaching profile. The compartmental model illustrated in Fig. 7B describes the dynamics of fluorescent biomolecules in a FRAP experiment when photobleaching a narrow band in the center of the nucleus. The model can be written as a system of ordinary differential equations, as follows:

$$\begin{aligned}
\dot{u}_0^f &= -2D_1u_0^f + D_2u_1^f + D_2u_2^f - k_au_0^f + k_du_0^b,\\
\dot{u}_1^f &= D_1u_0^f - D_2u_1^f - k_au_1^f + k_du_1^b,\\
\dot{u}_2^f &= D_1u_0^f - D_2u_2^f - k_au_2^f + k_du_2^b,\\
\dot{u}_0^b &= k_au_0^f - k_du_0^b,\\
\dot{u}_1^b &= k_au_1^f - k_du_1^b,\\
\dot{u}_2^b &= k_au_2^f - k_du_2^b,
\end{aligned} \tag{16}$$

where $\dot{u}$ denotes the derivative of with respect to time t, u_0^f, u_1^f, and u_2^f represent the population of diffusing fluorescent molecules in C_0, C_1, and C_2, respectively; u_0^b, u_1^b, and u_2^b represent the population of fluorescent molecules bound to the immobile structure in C_0, C_1, and C_2, respectively; k_a is the rate of association of molecules to the immobile structure; k_d is the rate of dissociation of molecules from the structure; D_1 is the fractional diffusional transfer coefficient from compartment C_0 to C_1 or C_2; and D_2 is the fractional diffusional transfer coefficient from compartments C_1 and C_2 to compartment C_0.

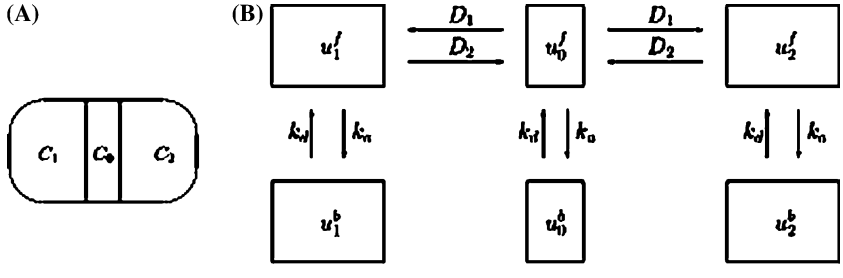

Fig. 7. (A) The three physical compartments of the cell nucleus during a FRAP experiment. C_0 is the photobleached band, and C_1, C_2 are the left and right unbleached regions respectively. (B) Compartmental model describing the dynamics of diffusing fluorescent biomolecules, that undergo binding and unbinding events, during a FRAP experiment when photobleaching a narrow band in the center of the nucleus. u_0^f, u_1^f, and u_2^f represent the population of diffusing fluorescent molecules in C_0, C_1, and C_2, respectively; u_0^b, u_1^b, and u_2^b represent the population of fluorescent molecules bound to an immobile structure in C_0, C_1, and C_2, respectively; k_a and k_d are the association and dissociation rates; and D_1 and D_2 are the fractional diffusional transfer coefficients.

Assuming that the diffusion properties of the biomolecules are independent of the physical compartment in which they are located, the fractional diffusional transfer coefficients D_1 and D_2 can be related to each other by a proportionality constant describing the relative sizes of the compartments or, equivalently, their relative fluorescence. If we denote the total fluorescence in the nucleus before photobleaching by F_0, and the fluorescence in the nucleus immediately after photobleaching by F_a, then the fluorescence in the photobleached compartment C_0 before photobleaching is $F_0 - F_a$, whereas it is $F_a/2$ in each of the unbleached compartments C_1 and C_2. Thus, D_1 and D_2 can described in terms of only one parameter D_t, called diffusional transfer coefficient, and in terms of F_0 and F_a as follows:

$$\begin{aligned} D_1 &= \frac{F_a/2}{F_a/2 + F_0 - F_a} D_t = \frac{F_a}{2F_0 - F_a} D_t, \\ D_2 &= \frac{F_0 - F_a}{F_a/2 + F_0 - F_a} D_t = 2\frac{F_0 - F_a}{2F_0 - F_a} D_t. \end{aligned} \tag{17}$$

Thus, there are three unknown parameters to be estimated, namely, D_t, k_a, and k_d. Note that $D_1 + D_2 = D_t$, which explains the use of the terms "fractional diffusional transfer coefficients" for D_1 and D_2 and "diffusional transfer coefficient" for D_t.

To obtain an initial condition for solving Eq. (16), we assume that the photobleaching is performed on an equilibrium state $\boldsymbol{u} = (u_0^f, u_1^f, u_2^f, u_0^b, u_1^b, u_2^b)$ that satisfies $u_0^f + u_1^f + u_2^f + u_0^b + u_1^b + u_2^b = 1$. So, the initial condition that reflects the experimental setting is given by

$$u_0 = \left(0, \frac{k_d}{k_a + k_d}\frac{F_a}{2F_0}, \frac{k_d}{k_a + k_d}\frac{F_a}{2F_0}, 0, \frac{k_a}{k_a + k_d}\frac{F_a}{2F_0}, \frac{k_a}{k_a + k_d}\frac{F_a}{2F_0}\right). \tag{18}$$

Using relations (17) and the initial condition (18) to solve Eq. (16), which following theoretical fluorescence recovery curve, which can be used to fit the experimental data $\overline{F}(t_j)$, is obtained:

$$R(t; \alpha, \beta, \gamma) = 1 - \gamma \exp(\alpha t) - (1 - \gamma)\exp(\beta t), \tag{19}$$

where α, β, and γ are nonlinear functions of D_t, k_a, and k_d. More concretely,

$$\begin{aligned} \alpha &= -S_1 + S_2, \\ \beta &= -S_1 - S_2, \end{aligned} \tag{20}$$

with

$$\begin{aligned} S_1 &= \frac{[(k_a + k_d)(2F_0 - F_a) + 2DF_0]}{2(2F_0 - F_a)}, \\ S_2 &= \frac{\sqrt{[(k_a + k_d)(2F_0 - F_a) + 2DF_0]^2 - 8(2F_0 - F_a)F_0 k_d D}}{2(2F_0 - F_a)}, \end{aligned} \tag{21}$$

and

$$\gamma = \frac{1}{2}\frac{k_d}{k_a + k_d}\Gamma_1\Gamma_2, \tag{22}$$

where

$$\begin{aligned} \Gamma_1 &= 1 + \frac{(2F_0 - F_a)(S_1 - S_2) + (2F_0 - F_a)k_a + 2DF_0}{k_d(2F_0 - F_a)}, \\ \Gamma_2 &= \frac{(2F_0 - F_a)(S_1 + S_2) - 2DF_0}{(2F_0 - F_a)S_2}. \end{aligned} \tag{23}$$

Note that Eq. (19) is expressed in terms of three new parameters, namely, α, β, and γ, but the parameters to be estimated are D_t, k_a, and k_d. The procedure for the parameter estimation is to estimate first α, β, and γ using the method of least squares [18], obtain an estimation for S_1 and S_2 from Eq. (20), and then solve, with any numerical scheme, the system of nonlinear equations given by Eqs. (21) and (22) to obtain the estimation of D_t, k_a, and k_d.

The fact that Eq. (19) is a simple exponential sum greatly simplifies the task of estimating parameters. Moreover, if the FRAP recovery curve exhibited slow and fast phases, this behavior would be satisfactorily explained by Eq. (19).

The estimation of association and dissociation (binding and unbinding) rates enables one to extract biological meaningful information, such as:

- $\tau_r = 1/k_d$: the average residency time of biomolecules in bound form;
- $\tau_w = 1/k_a$: the average wandering time of biomolecules between binding events;
- $P_b = k_a/(k_a + k_d)$: the steady-state proportion of biomolecules in bound form;
- $P_u = k_d/(k_a + k_d)$: the steady-state proportion of biomolecules in unbound form.

We have successfully applied the compartmental model Eq. (16) in the context of nuclear GFP–actin dynamics during FRAP experiments, explaining satisfactorily the fast and slow phases of the experimental fluorescence recovery data (manuscript in preparation). The same relevant information found for cytoplasmic actin using the reaction–diffusion model Eq. (15) in [20] was also obtained for nuclear actin using the compartmental model Eq. (16), namely, the average residency time of actin molecules in a filamentous form, and the proportion of actin molecules in monomeric and filamentous forms.

4. Concluding remarks

Fluorescence recovery after photobleaching and the accompanying mathematical analysis are becoming increasingly useful tools for studying the properties of proteins within living cells and cellular compartments. FRAP experiments have revealed the dynamic nature of some molecules and the surprisingly static nature of others. Although an energy-independent random walk diffusive motion is a common if not ubiquitous mechanism of moving cellular proteins around the cell, binding

events dominate the observed mobility of most nuclear proteins, resulting in a significant reduction in the apparent mobility or *effective diffusion coefficient* relative to the expected mobility for similarly sized inert molecules. Through the combined use of engineered proteins that dissect the contributions of individual molecular binding domains to the endogenous movement of individual proteins and increasingly sophisticated mathematical models, FRAP will likely remain an important tool in the arsenal of both the biochemist and the cell biologist for the foreseeable future.

Acknowledgments

The authors thank Dr. K.P. Hadeler (University of Tübingen) for valuable discussion on compartmental modeling. Original experimental work was supported by the Canadian Institutes of Health Research (M.J.H.). M.J.H. is supported by scholarship awards from the Canadian Institutes of Health Research and the Alberta Heritage Foundation for Medical Research. Theoretical work was supported by MITACS, a Canadian Network of Centres of Excellence (G.C.), and the Natural Sciences and Engineering Research Council of Canada (G.C. and G.deV.).

References

[1] A.B. Houtsmuller, W. Vermeulen, Histochem. Cell Biol. 115 (2001) 13–21.
[2] A.S. Verkman, Trends Biochem. Sci. 27 (2002) 27–33.
[3] T. Pederson, FASEB J. 13 (Suppl 2) (1999) S238–S242.
[4] J. Lippincott-Schwartz, E. Snapp, A. Kenworthy, Nat. Rev. Mol. Cell Biol. 2 (2001) 444–456.
[5] J. Ellenberg, J. Lippincott-Schwartz, Methods 19 (1999) 362–372.
[6] T. Misteli, Science 291 (2001) 843–847.
[7] T. Pederson, Nat. Cell Biol. 2 (2000) E73–E74.
[8] T. Pederson, Cell 104 (2001) 635–638.
[9] A.S. Verkman, Diffusion Measurements by Photobleaching Recovery Methods, Oxford University Press, 2001.
[10] N. Klonis, M. Rug, I. Harper, M. Wickham, A. Cowman, L. Tilley, Eur. Biophys. J. 31 (2002) 36–51.
[11] R.D. Phair, T. Misteli, Nat. Rev. Mol. Cell Biol. 2 (2001) 898–907.
[12] J. Ellenberg, E.D. Siggia, J.E. Moreira, C.L. Smith, J.F. Presley, H.J. Worman, J. Lippincott-Schwartz, J. Cell Biol. 138 (1997) 1193–1206.
[13] O. Seksek, J. Biwersi, A.S. Verkman, J. Cell Biol. 138 (1997) 131–142.
[14] A.B. Houtsmuller, S. Rademakers, A.L. Nigg, D. Hoogstraten, J.H. Hoeijmakers, W. Vermeulen, Science 284 (1999) 958–961.
[15] M. Wachsmuth, W. Waldeck, J. Langowski, J. Mol. Biol. 298 (2000) 677–689.
[16] D. Axelrod, D.E. Koppel, J. Schlessinger, E. Elson, W.W. Webb, Biophys. J. 16 (1976) 1055–1069.
[17] R.D. Phair, T. Misteli, Nature 404 (2000) 604–609.
[18] R.H. Myers, Classical and Modern Regression with Applications, Duxbury Press, Boston, 1986.
[19] K.J. Angelides, L.W. Elmer, D. Loftus, E. Elson, J. Cell Biol. 106 (1988) 1911–1925.
[20] Y. Tardy, J.L. McGrath, J.H. Hartwig, C.F. Dewey, Biophys. J. 69 (1995) 1674–1682.
[21] J.L. McGrath, Y. Tardy, C.F. Dewey Jr., J.J. Meister, J.H. Hartwig, Biophys. J. 75 (1998) 2070–2078.
[22] J. Crank, The Mathematics of Diffusion, Oxford University Press, London, 1975.
[23] P.A. Tavormina, M.G. Come, J.R. Hudson, Y.Y. Mo, W.T. Beck, G.J. Gorbsky, J. Cell Biol. 158 (2002) 23–29.
[24] M.O. Christensen, H.U. Barthelmes, S. Feineis, B.R. Knudsen, A.H. Andersen, F. Boege, C. Mielke, J. Biol. Chem. 277 (2002) 15661–15665.
[25] J. Sloan-Lancaster, J. Presley, J. Ellenberg, T. Yamazaki, J. Lippincott-Schwartz, L.E. Samelson, J. Cell Biol. 143 (1998) 613–624.
[26] L. Trinkle-Mulcahy, J.E. Sleeman, A.I. Lamond, J. Cell Sci. 114 (2001) 4219–4228.
[27] E.A. Reits, A.M. Benham, B. Plougastel, J. Neefjes, J. Trowsdale, EMBO J. 16 (1997) 6087–6094.
[28] W. Rodgers, S.J. Jordan, J.D. Capra, J. Immunol. 168 (2002) 2348–2355.
[29] J. Essers, A.B. Houtsmuller, L. van Veelen, C. Paulusma, A.L. Nigg, A. Pastink, W. Vermeulen, J.H. Hoeijmakers, R. Kanaar, EMBO J. 21 (2002) 2030–2037.
[30] M.J. Kruhlak, M.A. Lever, W. Fischle, E. Verdin, D.P. Bazett-Jones, M.J. Hendzel, J. Cell Biol. 150 (2000) 41–51.
[31] D. Chen, S. Huang, J. Cell Biol. 153 (2001) 169–176.
[32] S. Snaar, K. Wiesmeijer, A.G. Jochemsen, H.J. Tanke, R.W. Dirks, J. Cell Biol. 151 (2000) 653–662.
[33] F.M. Boisvert, M.J. Kruhlak, A.K. Box, M.J. Hendzel, D.P. Bazett-Jones, J. Cell Biol. 152 (2001) 1099–1106.
[34] T. Misteli, A. Gunjan, R. Hock, M. Bustin, D.T. Brown, Nature 408 (2000) 877–881.
[35] M.A. Lever, J.P. Th'ng, X. Sun, M.J. Hendzel, Nature 408 (2000) 873–876.
[36] H. Kimura, P.R. Cook, J. Cell Biol. 153 (2001) 1341–1353.
[37] B.F. Lillemeier, M. Koster, I.M. Kerr, EMBO J. 20 (2001) 2508–2517.
[38] D.L. Stenoien, K. Patel, M.G. Mancini, M. Dutertre, C.L. Smith, B.W. O'Malley, M.A. Mancini, Nat. Cell Biol. 3 (2001) 15–23.
[39] M.J. Hendzel, M.J. Kruhlak, N.A. MacLean, F. Boisvert, M.A. Lever, D.P. Bazett-Jones, J. Steroid Biochem. Mol. Biol. 76 (2001) 9–21.
[40] J.G. McNally, W.G. Muller, D. Walker, R. Wolford, G.L. Hager, Science 287 (2000) 1262–1265.
[41] E.R. Griffis, N. Altan, J. Lippincott-Schwartz, M.A. Powers, Mol. Biol. Cell 13 (2002) 1282–1297.
[42] N. Daigle, J. Beaudouin, L. Hartnell, G. Imreh, E. Hallberg, J. Lippincott-Schwartz, J. Ellenberg, J. Cell Biol. 154 (2001) 71–84.
[43] E.S. Scott, P. O'Hare, J. Virol. 75 (2001) 8818–8830.
[44] C. Ostlund, J. Ellenberg, E. Hallberg, J. Lippincott-Schwartz, H.J. Worman, J. Cell Sci. 112 (Pt 11) (1999) 1709–1719.
[45] S.B. Martins, T. Eide, R.L. Steen, T. Jahnsen, B.S. Skalhegg, P. Collas, J. Cell Sci. 113 (Pt 21) (2000) 3703–3713.
[46] R.D. Moir, M. Yoon, S. Khuon, R.D. Goldman, J. Cell Biol. 151 (2000) 1155–1168.
[47] C.L. Wey, R.A. Cone, M.A. Edidin, Biophys. J. 33 (1981) 225–232.